Chapter 4

Magnetization dynamics of soft nanocrystalline thin films with random magnetocrystalline anisotropy and induced uniaxial anisotropy

Results of frequency-dependent ferromagnetic resonance (FMR) measurements are presented for thin Fe-Zr-N nanocrystalline films with random magnetocrystalline anisotropy and induced uniaxial anisotropy. The study is done by changing the composition, the grain size and the magnitude of the induced anisotropy. We show that the magnetization dynamics is strongly influenced by the structural parameters of our samples. Although the frequency-dependent spectra can be analyzed on the basis of the Landau-Lifshitz equation, an extra field H_{shift} has to be introduced in order to have agreement between the experiment and calculations. This extra field does not depend on the saturation magnetization and increases significantly when the grain size decreases from 10 to 2 nm. In addition, we observe a nonlinear decrease of the frequency linewidth with the applied DC field. After discussing various existing models we conclude that H_{shift} originates from variations in the *magnitude* of the magnetization, related with the nanocrystalline stucture.

4.1. Introduction

Recently, nanocrystalline ferromagnetic materials with random orientation of the grains and induced uniaxial anisotropy were recognised as potential candidates for integration in high frequency applications [1, 2]. In this respect, the most relevant quantity is the frequency-dependent complex permeability, the real part of which should be sufficiently high up to GHz frequencies.

In nanocrystalline ferromagnetic materials, the magnitude of the local anisotropy field H_r determines the nature of the magnetic response of the system. When H_r is larger than the exchange field H_{ex} the spins are directed along the local anisotropy axis. In this case, although there is a small magnetic correlation length, the collective behavior is only of minor importance. If $H_r < H_{ex}$ then the grain size, the external applied field and the induced anisotropy field will determine the collective behavior of the system [3]. In this chapter we will discuss only the last category.

A small applied field or a coherent anisotropy field will be sufficient to nearly align the spins of the system. The magnetic structure is also called ferromagnet with wandering axis (FWA). The deviation angle from the average orientation of magnetization is correlated over a certain field-dependent length which depends on the external applied field and the magnitude of the coherent uniaxial anisotropy, if present.

As part of our structural and magnetic studies of the Fe-Zr-N system [4-6], we present here an investigation of the magnetization dynamics as a function of an external magnetic field H_{DC}, applied in the plane of the samples. The samples were oriented with the easy axis (*EA*) parallel or perpendicular to H_{DC}. We discuss the transversal resonance mode in relation with composition, grain size and magnitude of induced anisotropy field of our samples.

4.2. Experimental

The samples were obtained by DC reactive sputtering in an $Ar+N_2$ gas mixture. The targets were prepared in order to have atomic concentration ratios between Zr and Fe of 0.01, 0.025 and 0.04. A sample holder with a controlled temperature between –55°C and +220°C was used. By controlling the temperature of the substrate we can influence structural properties like grain size and nitrogen content [7]. The sputtering power was 10 W, ensuring a deposition rate of 5 Å/s. A constant DC field of 600 Oe was applied parallel to the plane of the sample to confine the plasma and to induce an uniaxial anisotropy. Quantitative estimations of grain size and nitrogen content were done using X-ray Diffraction (XRD) θ-2θ scans. As we have found [8] the nitrogen content correlates with the lattice parameter and thus with the position of the Bragg reflection. In Chapter 2 it was discussed that the grain size

can be estimated from the width of the Bragg peak. The thicknesses of the samples were determined using the Rutherford Back Scattering (RBS) technique.

We present in the Table 4.1 the structural parameters of the samples of this study. As expected, the grain size and nitrogen content correlate with the temperature of the substrate. When the substrate temperature was low, the grain size was small and the nitrogen content was high. Samples with larger grains and lower concentration of nitrogen were obtained at high temperatures. These effects are related with the mobility of the atomic species during deposition. We note that the grain size is significantly smaller than the ferromagnetic correlation length (≅35nm), so that we are in the situation that the direction of the local magnetization, averaged over an exchange coupled volume, makes small excursions from the average direction (FWA regime).

The DC magnetic properties were investigated with a Vibrating Sample Magnetometer (VSM). As a common feature, all samples showed almost rectangular hysteresis loops measured in the direction parallel to the easy axis, proving that at the remanence we have a single-domain magnetic structure. The values of the coercive field were in the range of 1÷10 Oe for the easy axis orientation and 1.5÷5 Oe for the hard axis orientation.

Sample name	Zr at.%	*T* (°C)	<*D*> (nm)	*t* (nm)
A1	1	-30	2	50
A2	1	200	13	60
B1	2.5	-55	1	100
B2	2.5	207	11	100
C1	4	-64	2	100
C2	4	215	7	100

Table 4.1

Characteristics of the sputter-deposited samples. The various columns give the Zr content, the substrate temperature T, the average grain size <D> and the layer thickness t.

The magnetization dynamics was studied using a copper single coil connected to a Network Analyzer (HP8720A and HP8720S). The frequency band for which we have designed the device was from 130 MHz up to 6 GHz. By measuring the reflection parameter S11 of the single coil, the complex permeability can be obtained from an appropriate analytical description of the device [9]. We refer to

Chapter 2 for details. A proper subtraction of the substrate signal was done by orienting the sample with the magnetization parallel to the orientation of the RF field. In this case the magnetic response vanishes. All measurements with this technique were done with the external applied field and RF field aligned in the plane of the sample. We have also measured the FMR response in the X band (9.4 GHz) with a standard electron spin resonance (ESR) spectrometer.

4.3. Frequency dependent permeability

Here we discuss the suitability of the description given by the Landau-Lifshitz (L-L) equation as a phenomenological approach. Although the equation was initially written for coherent rotations of the spins, we will show that it describes the frequency-dependent permeability of our samples fairly well. Because this equation is nonlinear, it is difficult or impossible to solve it for the general case. Using reasonable assumptions [10] for the highly permeable films we can approximate the equation by a linear one. The assumptions are: i) the anisotropy field is small in comparison with the saturation magnetization; ii) the RF field is small so that the tipping of the magnetization is negligible, iii) the damping constant α is small; iv) the film is so thin that eddy currents can be neglected; v) if an external DC field H_{DC} is applied, then its value has to be large enough so that the magnetization is parallel to it. This implies that for the case that the RF field is in the direction of H_{DC} (and thus in the direction of the magnetisation) the RF magnetic response is zero. As discussed in Chapter 2 we used this in the calibration of our impedance analyser.

Neglecting the terms of order higher than α^2, the general form of the L-L is:

$$\frac{d\boldsymbol{M}}{dt} = \gamma\left(\boldsymbol{M}\mathrm{x}\boldsymbol{H}_{\boldsymbol{eff}}\right) - \frac{\alpha}{M}\boldsymbol{M}\mathrm{x}\left[\frac{d\boldsymbol{M}}{dt} + \frac{\alpha}{M}\left(\boldsymbol{M}\mathrm{x}\frac{d\boldsymbol{M}}{dt}\right)\right] \tag{4.1}$$

where $\boldsymbol{M}$ is the magnetization, $\boldsymbol{H}_{\boldsymbol{eff}}$ the effective field, $\gamma = \frac{g\mu_B}{\hbar}$ is the gyromagnetic ratio (μ_B is the Bohr magneton). The external RF field is taken as $\boldsymbol{H}_{RF}(t) = \boldsymbol{H}_{RF0}e^{i\omega t}$. With these considerations, we can write the magnetization and the effective field as follows:

$$\begin{aligned} \mathbf{M} &= \mathbf{M}_{\mathbf{S}} + \mathbf{m}(t) \\ \mathbf{H}_{\mathbf{eff}} &= \mathbf{H}_{DC} + \mathbf{H}_{RF}(t) - \mathbf{H}_{dem} + \mathbf{H}_{k} \end{aligned} \tag{4.2}$$

where **m**(t) is the magnetisation due to the RF field, $\boldsymbol{H}_{dem}$ is the demagnetizing field and $\boldsymbol{H}_k$ is the anisotropy field. The magnetization is along the *OX* axis and $\boldsymbol{H}_{dem}=(0,4\pi M_S,0)$.

By inserting equation (4.2) in equation (4.1) we obtain the simplified expression for the component μ_{xx} of the complex permeability tensor in two geometries:

a) $\boldsymbol{H}_{RF}||HA$ (hard axis), which is equivalent to $\boldsymbol{H}_{DC}||EA$ (easy axis), with $\boldsymbol{H}_{RF}$ in the plane of the sample:

$$\mu_{\mathrm{Hrf||HA}} = \frac{(4\pi M_S)^2}{(H_{DC}+4\pi M_S)(H_{DC}+H_K)-\frac{\omega^2}{\gamma^2}+i\Gamma 4\pi M_S}+1 \tag{4.3a}$$

b) $\boldsymbol{H}_{RF}||EA$, equivalent to $\boldsymbol{H}_{DC}||HA$:

$$\mu_{\mathrm{Hrf||EA}} = \frac{(4\pi M_S)^2}{(4\pi M_S+H_{DC}-H_K)(H_{DC}-H_K)-\frac{\omega^2}{\gamma^2}+i\Gamma 4\pi M_S}+1 \tag{4.3b}$$

where $\Gamma = \dfrac{\alpha\omega}{\gamma}$.

We note that formulas (4.3a,b) are valid only if $H_{DC} \ll 4\pi M_S$, a proper assumption for our data on the frequency dependent permeability.

All spectra can be fitted in a good agreement with Eq. 4.3, for an example see Fig. 4.1. The resonance frequencies follow directly from the resonance condition of Eqs. 4.3a and 4.3b:

$$f_{H_{RF}||HA} = \frac{\gamma}{2\pi}\sqrt{(H_{DC}+4\pi M_S)(H_{DC}+H_K)} \tag{4.4a}$$

$$f_{H_{RF}||\mathrm{E}A} = \frac{\gamma}{2\pi}\sqrt{(H_{DC}-H_K+4\pi M_S)(H_{DC}-H_K)} \tag{4.4b}$$

These expressions are also valid for the ferromagnetic resonance at 9.4 GHz, because here we have $H_{DC} \gg H_K$.

There are three major conclusions of this investigation which will be discussed in the next sections: (i) for the samples with a well defined induced anisotropy the line shape is lorentzian, indicating a purely relaxation-type process, (ii) the ferromagnetic resonance line position is shifted towards higher frequency values than given by Eq. 4 and (iii) the phenomenological damping parameter has a pronounced nonlinear behavior as a function of the external applied field.

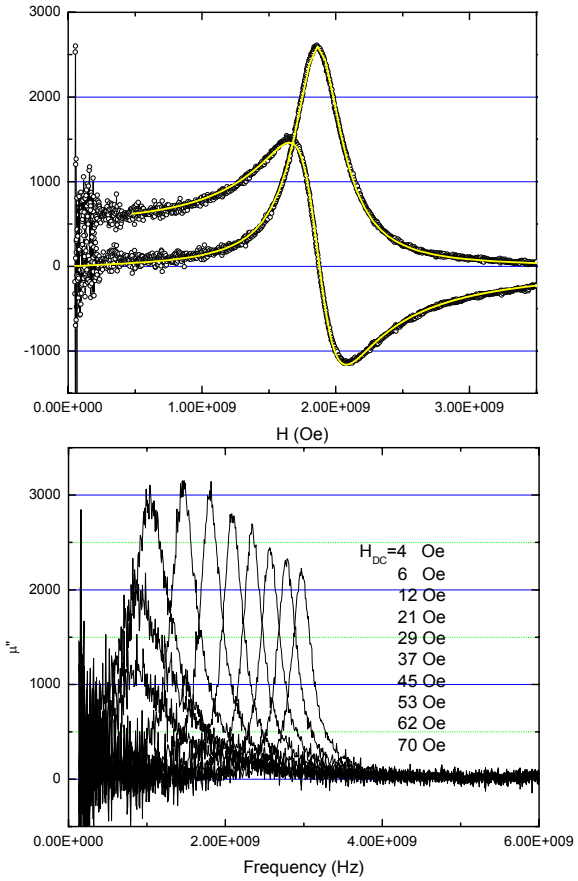

Fig. 4.1

a. The permeability spectra for the sample B1: experimental measurement – circle; L-L fit –line.
b. Imaginary part of the complex permeability of the sample C2; geometry $H_{RF}||EA$. The values of H_{DC} correspond to spectra from left to right.

4.4. Results

4.4.1. X-band ferromagnetic resonance

Before presenting our experimental results concerning the induced anisotropy field and the shift of the ferromagnetic resonance frequency, it is essential to determine the saturation magnetization. This is done from the in-plane FMR field-dependent measurements, see results in Table 4.2. In these estimations we have taken the *g* factor as for pure Fe, *g*=2.1 [11]. We could determine the *g* value for sample C1 (with the highest Zr concentration and nitrogen content) from the FMR with perpendicular and parallel field orientation with respect to the sample surface. For the former geometry the resonance frequency is:

$$f_{\perp} = \frac{\gamma}{2\pi}\left(H_{\perp} - 4\pi M_S\right) \tag{4.5}$$

where $H_{\perp}$ is the corresponding resonant field. The above formula is valid when the perpendicular component of the anisotropy is insignificant, like in our case.

Combining Eq.4 and 5 we can obtain the g value independent of M_S. The result was g=2.051(±0.003). Unfortunately the maximum value of the field, possible to reach in our ESR set-up, has limited this type of measurements to only one sample. Because the sample C1 contained the maximum concentration of Zr, we assume that the g value for the other samples is closer to 2.10. We conclude that taking g=2.10 for all samples may underestimate M_S by 5% at maximum. Because the samples contained a high degree of imperfections like vacancies and voids, the evaluation of their volume has an uncertainty of 10%. Since the magnetization is the ratio between

Sample	<D> (nm)	N (at. %)	$4\pi M_S$ (kG)	H_K (fr.) (Oe)	H_K (field) (Oe)	H_{shift} (Oe)
A1	2	14	16.9	23.8(±0.2)	25(±2)	7.3(±0.3)
A2	13	2	19.1	1.5(±0.2)	0(±2)	0(±0.2)
B1	1	11.5	15.7	16.7(±0.3)	18(±2)	6.4(±0.3)
B2	11	7	17.1	5.3(±0.1)	9(±2)	3.3(±0.1)
C1	2	12	13.4	15.3(±0.2)	13(±2)	7.3(±0.3)
C2	7	6	15.9	6.2(±0.1)	7(±2)	1.6(±0.1)

Table 4.2. Saturation magnetization $4\pi M_S$, anisotropy field as determined by frequency-dependent measurements: H_K (fr.) and by X-band FMR: H_K (field), and the additional field H_{shift} acting on the spins. Also average grain size <D> and nitrogen content are given.

the magnetic moment and the sample volume the error bar as determined from VSM measurements is then also 10%.

Standing spin waves (SSW) were excited in spectra measured with H_{DC} perpendicular to the plane, see Fig. 4.2a. A quadratic dependence of the line positions $H_n = H_0 - D_b\left(\frac{n\pi}{t}\right)^2$ on the mode number n is expected if the following conditions are met: (i) the spins are pinned at the surface, (ii) the exchange coupling constant, the internal static field and the RF field are homogenous inside the sample, (iii) the sample is saturated and there is no perpendicular component of the coherent anisotropy. D_b is called the *bulk* exchange stiffness constant of the film. For our experimental results, the closest line-indexing to a quadratic dependence is found when the second line has n=2, the third line n=3 and the fourth line n=4. Although the resolution should be sufficient, the line corresponding to the mode number n=1 was

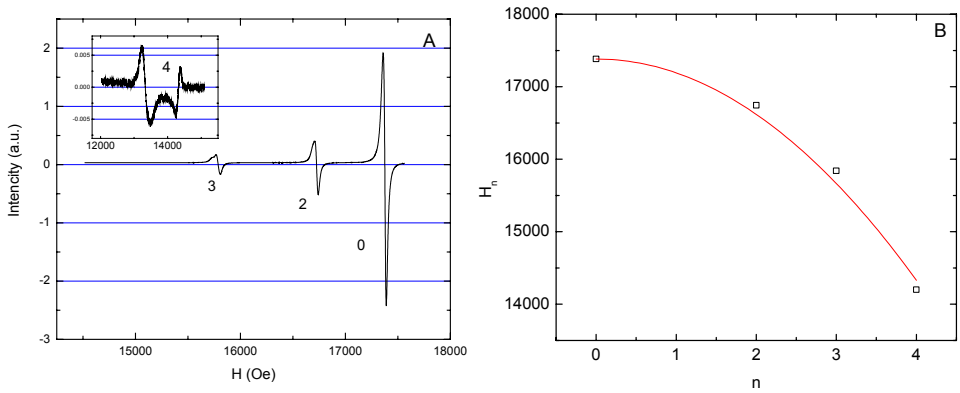

Fig. 4.2 Sample C1: a) Standing spin waves spectra; b) Resonance field versus resonance mode: squares - experimental points ; line – simulation with the formula $H_n = H_0 - D\left(\frac{\pi n}{t}\right)^2$

not observed. The experimental field ratios are $(H_0 - H_2)/(H_0 - H_3) = 0.41$, $(H_0 - H_2)/(H_0 - H_4) = 0.20$, $(H_0 - H_3)/(H_0 - H_4) = 0.47$ and have to be compared with 0.44, 0.25, 0.56 as expected for a quadratic behavior. A fit of D_b based on the above model leads to D_b=1.93 10^{-9}Oe cm^2, see Fig. 4.2b. This value can be compared with the experimental value of pure Fe [12] $D_{b\text{-}Fe}$=2.34 10^{-9} Oe cm^2. We conclude that the standing wave patterns we observe cannot be described accurately by the simple model given above. The most obvious flaw of this model is the neglect of the nanocrystalline structure of our material. Within the grains the exchange constant is probably bigger than in the defected interface regions. This will lead to a complicated magnon spectrum. We note that other authors have associated the standing wave parameters with the structural correlation length [13].

4.4.2. Induced anisotropy field

In Fig. 4.3a.b. we present the square of the FMR frequency as a function of H_{DC} for the samples C1 and C2. Similar data was extracted for all samples. The external field used (H_{DC}< 70 Oe) as well as the anisotropy field H_K are very small compared to the saturation magnetization and consequentely can be neglected in the first factor under the square root in Eq. 4a,b. The slope of the graphs is consistent with the values of M_S and g calculated from the ferromagnetic resonance measurements at 9.4 GHz. Contrary to what is expected from Eq. 4a,b, the lines do not cross the horizontal axis at the same distance to the origin and the FMR frequency for $H_{RF}||EA$ does not reach zero value.

From the resonance conditions of both $H_{RF}||HA$ and $H_{RF}||EA$, we find the dependence of H_K on the difference between the squares of the FMR frequencies:

$$H_K \cong \frac{c}{8\pi M_S}, \tag{4.6}$$

where $c = \frac{f_{HA}^2 - f_{EA}^2}{(2\pi\gamma)^2}$. HA and EA are the indices of the corresponding ferromagnetic resonance frequencies as measured for the same applied field. The values for H_K derived in this way for the samples C1 and C2 are given in Fig. 4.3c.

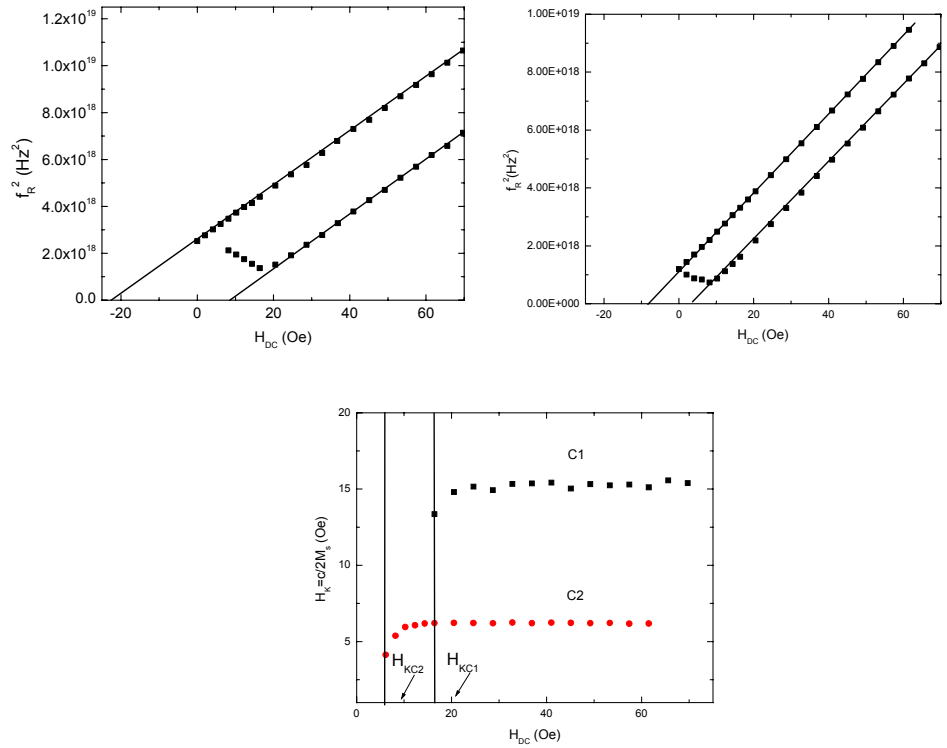

Fig. 4.3 a,b)The square of the resonance frequency versus H_{DC} of the sample C1 and C2; c) Uniaxial anisotropy field of samples C1 and C2 measured in an external field from 0 to 70 Oe.

We see that H_K is independent of H_{DC}, apart from the region where H_{DC} is close to H_K. In this case the torque on the spins is very small for the configuration "EA" and any inhomogeneity in the sample will result in a more complicated behavior of the local magnetization. These values correlate with the nitrogen concentration and with the average grain size <D>. The origin of the induced anisotropy lies in the anisotropic distribution of N atoms in planes perpendicular to the external field applied during deposition [14]. Similar results for H_K were obtained from FMR measurements done by sweeping the magnetic field. However, the error bars of H_K as

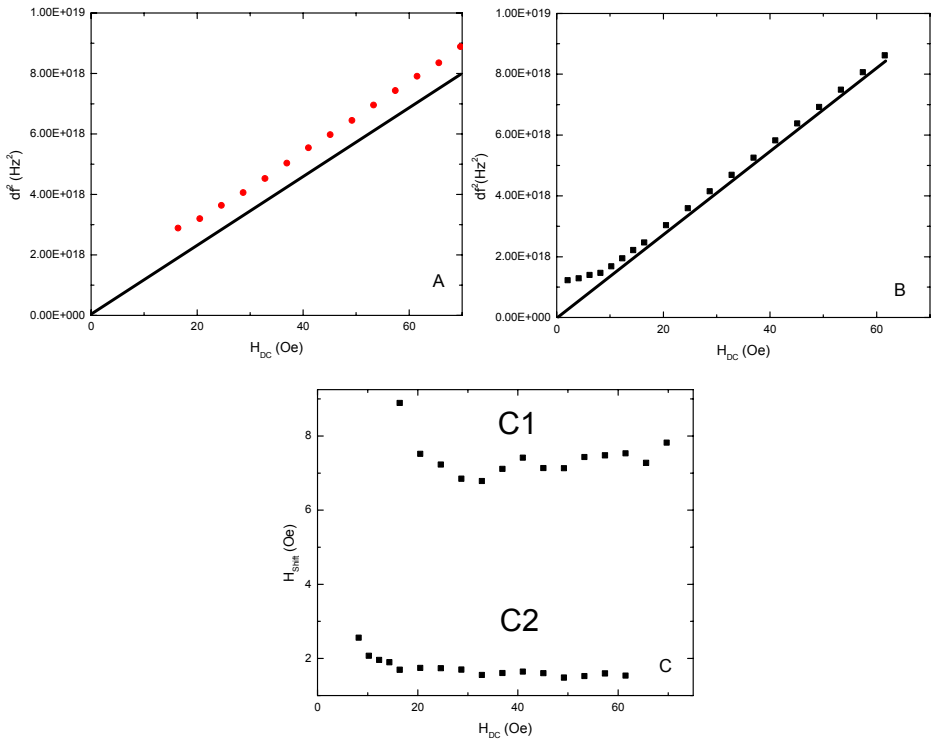

Fig.4.4. The average of the FMR frequencies for the sample C1 (a) and C2(b), measured at the same external field for two geometries; (c) H_{shift} extracted from (a) and (b)

determined with last mentioned technique are larger by a factor of 10 as compared with the magnitude of H_K of the samples with small nitrogen content. We conclude that the frequency sweep method is more appropriate for anisotropy field determinations.

For the regime where H_{DC} is sufficiently larger than H_K, so that magnetization is everywhere parallel to H_{DC} we observe that both H_K and H_{Shift} are independent of H_{DC}. We present in Table 4.2 the H_{Shift} values for this regime. For the samples produced at low temperature, the grain size D is small, the N concentration is large, and both H_K and H_{Shift} are large. For the samples made at ~ 200ºC we have larger grains, lower nitrogen content and small values for H_K and H_{Shift}. The best correlation is between nitrogen content and H_{Shift}, see Fig. 4.5. On the other hand, M_S seems to have little influence on H_{Shift} (compare samples A1, B1 and C1).

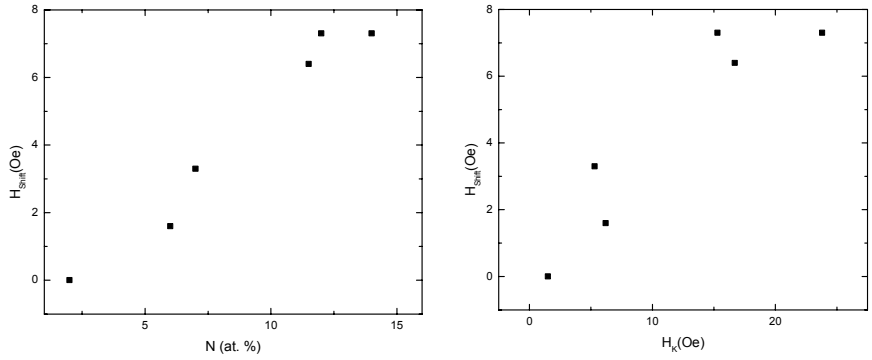

Fig. 4.5 (a) H_{Shift} versus N content and (b) H_{Shift} versus H_K.

4.4.3. Line broadening

In this section we discuss the ferromagnetic resonance line width as a function of the external applied field. All samples showed similar behavior to the one in Fig. 4.6. The largest linewidth is observed for $H_{RF}||EA$ when the external field is almost equal to the anisotropy field. In these conditions, the resulting torque on the spins is very small which makes the system very sensitive to fluctuations. As expected, the fluctuations are most prominent for larger grains. However, we observe that while H_{Shift} goes almost immediately constant when H_{DC} is above this region, the linewidth decreases more slowly with H_{DC}.

In order to extend this investigation to higher values of H_{DC} we present in Table 4.3 the maximum value of the frequency linewidth, the value at 60 Oe and the value derived from the FMR measurements at 9.4 GHz. The line width seems to approach a constant value at fields higher than H_K but in fact a further decrease takes place going to 9.4 GHz. This is quite different from what is observed in a classical soft material like permalloy. In that case the damping parameter α is field independent, leading to a linear but weak dependence of the linewidth with the DC field in accordance with:

$$\Delta\omega = \alpha\gamma\left(2H_{DC}+4\pi M_S\right) \tag{4.7}$$

In contrast with these observations we measure a decrease of the line width with H_{DC}, as is evident from Fig. 4.6. Note that this figure also contains the point at 635 Oe, corresponding to f= 9.35 GHz. This can only be explained by a non-linear decrease of the damping parameter α with increasing H_{DC}. A similar nonlinearity of α was observed by Sun et all [14] on nanocrystalline Fe-Co-N thin films.

In Table 4.3 we can also see that the linewidth increases with M_S. This is predicted by Eq. 4.7 if we assume that the damping parameter does not depend on M_S. Indeed, for the last two columns of Table 4.3 the calculated values for α do not show a correlation with M_S. Likewise, we do not observe a clear influence of the grain size on the damping parameter.

From the FMR response measured in the X-band we have calculated the frequency linewidths $\Delta\omega_{\parallel,\perp}$ of sample C1, corresponding to H_{DC} parallel and perpendicular to the sample surface. The values were $\Delta\omega_{\parallel}$=160 MHz and $\Delta\omega_{\perp}$=100 MHz. The larger linewidth in the parallel case is usually associated with the presence of spin waves with energies equal to the uniform ferromagnetic resonance mode ($\boldsymbol{k}$=0), enabling a so-called two magnon process. This situation does not occur when the field is perpendicular to the sample surface[16, 17]. We will return to this point in the next section.

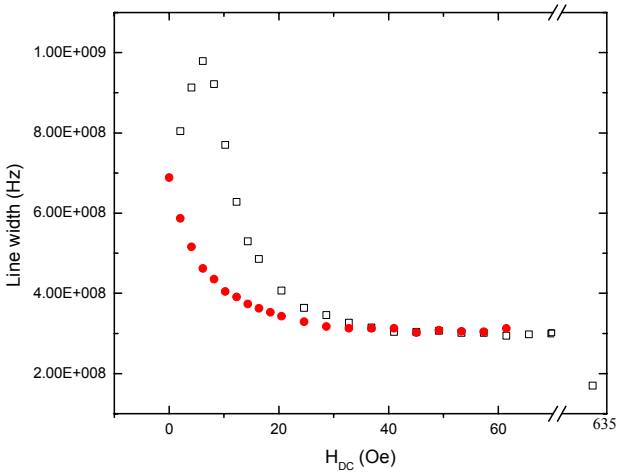

Fig. 4.6. The FMR linewidth for sample C2 as a function of the external field, in two different geometries: H_{RF}||EA (squares) and H_{RF}||HA (circles).

Sample	Zr (at.%)	D (nm)	$4\pi M_S$ (kG)	W_{max} (MHz)	$W_{60\ Oe}$ (MHz)	$W_{9.4GHz}$ (MHz)
A1	1	2	16.9	890	460	327
A2	1	13	19.1	1160	560	380
B1	2.5	1	15.7	630	380	195
B2	2.5	11	17.1	1000	440	205
C1	4	2	13.4	580	330	160
C2	4	7	15.9	980	300	170

Table 4.3 The maximum frequency linewidth (W_{max}), the frequency linewidth measured at 60 Oe ($W_{60\ Oe}$) and the calculated frequency linewidth from the in-plane field dependent measurements (W_{field}) versus grain size and Zr concentration.

4.5. Discussion

Several effects are present in nanocrystalline films with random anisotropy that may influence the magnetization dynamics. We will discuss them here in relation with the present findings: the existence of an extra field H_{Shift} acting on the spins and the peculiar behavior of the FMR linewidth.

4.5.1. Longitudinal stray fields due to magnetization fluctuations

Hoffmann has shown [18] that fluctuations present in the FWA regime are basically one-dimensional. In a plane perpendicular to the average magnetization direction (x-axis) the spins are practically parallel, but along the x-axis the direction of the magnetization fluctuates on a length scale larger than the ferromagnetic correlation length. This gives rise to a so-called ripple pattern, which has been observed in some of our samples by Lorentz microscopy [4]. This magnetization pattern leads to magnetic charge density varying along the x-axis. Coupled to this is a stray field (demagnetizing field) directed along the x-axis. As we have shown, this stray field distribution locally influences the magnetization dynamics, giving rise to a distribution of resonance frequencies [4]. For relatively large sinusoidal magnetization fluctuations, it leads to a double hump in the FMR response. Note, however, that our treatment does not lead to an average shift of the resonance frequency. Although we have observed these effects for samples deposited on rough substrates, where bumps and pits can lead to additional stray field distributions [19], this is not the case for the samples presented here.

On the basis of the treatment given by Hoffmann [18] we estimate that effects of the stray field distribution are negligible even for the samples with relatively large grains, except possibly for the region close to H_K in the EA

configuration, where the spin system is very susceptible to local inhomogeneities. In accordance with this estimate we do not see any deviation in the line shape behavior from the simple Landau-Lifshitz behavior (Eq. 3a and 3b).

4.5.2. Random anisotropy model

Saslow and coworkers have studied a microscopic model applicable to ferromagnetic systems with random anisotropy [20, 21]. In this model the spins are subject to various magnetic fields. Apart from a possible external field, one introduces a random anisotropy field H_r which is directly related to the local magnetocrystalline anisotropy energy, and an exchange field H_{ex} defined as $H_{ex}=Ja^2M_S/D^2$, where J is the exchange constant, a is the interatomic distance and D the characteristic length of the structural variations (i.e. the grain size). This treatment does lead to a shift in the dispersion curve of the excitations, implying also a shift in the ferromagnetic resonance frequency (transversal mode), for which one can write:

$$H_{Shift} = \frac{H_r^2}{3H_{ex}} \tag{4.8}$$

i.e. H_{Shift} is proportional to D^2.

Apart from the fact that numerical estimates give a small value for H_{Shift}, the D-dependence is completely different from what is observed experimentally, namely H_{Shift} *increases* for decreasing grain size.

4.5.3. Skew effect

The skew effect appears when we deal with a gradual variation in the orientation of the induced anisotropy, leading to a misalignment of the magnetization on length scales much larger than discussed before. In principle this can lead to an extra torque described by an effective field H_{Skew}. We can exclude such an effect in our samples for the following reasons: i) no magnetic response was observed in a geometry where H_{RF} was parallel to the average magnetization (easy axis) with no external field present, ii) the theoretical treatment of the skew effect [18] predicts $H_{Skew}\sim H_{DC}^{-1}$, which is not observed experimentally.

4.5.4. Variations in the magnitude of the magnetization

Although in our fine-grained samples the variation in magnetization direction is negligible because it costs too much exchange energy, the magnitude of the local magnetization will vary, mainly because the atom density in the intergranular region will be smaller than in the interior of the grains. This will lead to local demagnetizing fields that vary on a length scale comparable to the grain size. These fields will average out in the x-direction (parallel to the external field), but this is not the case for the z-direction (in the plane of the film). Consequently, the perpendicular magnetization component M_z is associated with a magnetostatic energy density $<(M_z - M_{av,z})^2>$ [22]. This is similar to the term $2\pi M_y^2$ for the magnetization component perpendicular to the plane.

Adapting a simple model due to Jamet and Malozemoff [23], we assume that the magnetization and the exchange stiffness vary as a sine wave in two dimensions, i.e.: $M(x,z) = M_0 + M_1 \sin(kx)\sin(kz)$ and $A(x,z) = A_0 + A_1 \sin(kx)\sin(kz)$, where $M_1 < M_0$ and $A_1 < A_0$; k is the wave vector corresponding to the magnetization periodicity. For our case, in which the wavelength $2\pi/k$ is much smaller than the exchange length and the static magnetization lies along the x-direction, the ferromagnetic resonance condition is given by:

$$\omega = \gamma \left[4M_0 \left(H_{static} + H_{loc}\right)^{1/2}\right] \tag{4.9}$$

where $H_{static} = H_{DC} \pm H_K$ and $H_{loc} = 2\pi M_1^2 / M_0 = \frac{1}{2} (4\pi M_1)^2 / 4\pi M_0$.

We conclude that we can associate our extra field H_{shift} with the term H_{loc}. With $H_{shift} = 7$ Oe and $4\pi M_0 = 17$ kOe we arrive at $4\pi M_1 \approx 5.\ 10^2$ G, or $M_1 / M_0 \approx 3\%$. Such a variation in the magnitude of $\boldsymbol{M}$ looks very reasonable. We further note that we can easily extend the model by assuming a distribution in the wave number k. As long as the corresponding wavelengths of the fluctuations are negligible compared to the exchange length (which is a reasonable assumption for our nanocrystalline material), the result is independent of k. The standard deviation of the magnetization distribution is then given by $\sqrt{\langle M_1^2 / 2 \rangle}$. The fact that we observe a bigger field shift for material with smaller grains and more nitrogen suggests that the atomic density variations between grains and intergranular region are larger in that case than for material with larger grains. This is understandable, because the volume fraction of the intergranular region is larger for smaller grains.

4.5.5. Spin wave excitations

The dispersion relation for spin waves (magnons) in a thin foil can be written as:

$$\omega_k^2 = \gamma^2 (H_i + Dk^2)(H_i + Dk^2 + 4\pi M_S^2 \sin^2\theta_k) \tag{4.10}$$

where D is the spin wave constant in frequency units and θ_k the angle between the magnetization and the propagation direction $\boldsymbol{k}/k$. This expression assumes a homogeneous and isotropic material, apart from the small induced anisotropy field. The effective field H_i is given by $H_i = H_{DC} \pm H_K$ when the external field is in the surface plane, parallel respectively perpendicular to the induced easy axis. On the other hand, when the external field is perpendicular to the plane and sufficiently large to magnetize the system in that direction, we have $H_i = H_{DC} - 4\pi M_S$.

If we compare these expressions with the corresponding FMR frequencies, i.e. the excitation frequencies for the $\boldsymbol{k}$=0 (uniform) magnon, we deduce that for an external field in the plane of the sample the energy of the $\boldsymbol{k}$=0 mode is at the top of the magnon band ($k\rightarrow 0$, θ_k=0) whereas for the perpendicular geometry the $\boldsymbol{k}$=0 mode lies at the bottom of the magnon band. This explains the presence of a two-magnon relaxation process for the parallel geometry, in which a k=0 magnon is destroyed and a magnon with the same energy, but $k\neq 0$, is created.

While this mechanism accounts for the larger linewidth when $\boldsymbol{H}_{DC}$ is parallel to the sample plane compared to $\boldsymbol{H}_{DC}$ perpendicular to the plane, it cannot explain the decrease of the linewidth as a function of H_{DC}, because –at least for the simple case expressed by eq. 10- the relative energies of the various magnons do not depend on the external field. Probably this decrease of the linewidth (or alternatively the damping parameter) is related to the fact that in our nanocrystalline material the exchange stiffness constant and the spin wave constant D, is position dependent. This will clearly influence the shape of the magnon spectrum and the possible relaxation channels.

4.6. Conclusions

The magnetization dynamics of nanocrystalline ferromagnetic films of the type Fe-Zr-N have been studied as a function of an in-plane external magnetic field H_{DC}, applied parallel as well as perpendicular to the easy axis. Grain size and concentration of Zr and N were varied by changing the deposition parameters. The complex permeability of all samples is well described by the Landau-Lifshitz-Gilbert equation. However, apart from the torques due to the external field and the uniaxial anisotropy, the spins experience an extra torque that can be described by an additional field H_{Shift}, independent of H_{DC}. H_{Shift} is larger for the samples with small grains and

seems to correlate with the amount of N in samples. The linewidth decreases as a function of H_{DC}, which also deviates from the behavior of classical soft ferromagnets (Permalloy). After discussing various models for magnetic systems with random anisotropy we conclude that the extra field is due to demagnetizing fields acting on the perpendicular component of the magnetization, as was described earlier by Jamet and Malozemoff. These fields are caused by variations of the magnitude of the magnetization related with the nanocrystalline nature of the material. The effect of spin wave excitations is also discussed; we argue that they do not provide an explanation of the behavior of the linewidth as a function of the external field.

References

1. S.X. Wang, N.X. Sun, M. Yamaguchi, S. Yabucami, Nature **407**, 150 (2000)
2. V. Korenivski and R.B. Dover, J. Appl. Phys. **82**, 5247 (1997)
3. F. Hellman, A.L. Shapiro, E.N. Abarra, R.A. Robinson, R.P. Hjelm, P.A. Seeger, J.J. Rhyne, J.I. Suzuki, Phys. Rev. B **59**, 11408 (1999)
4. N.G. Chechenin, C.B. Craus, A.R. Chezan, T. Vystavel, D.O. Boerma, J.Th.M. De Hosson and L. Niesen, IEEE Trans. on Mag. **38**, 3027 (2002);
5. A.R. Chezan, C.B. Craus, N.G. Chechenin, L. Niesen and D.O. Boerma, Phys. Stat. Sol. A **189**, 833 (2002)
6. C.B. Craus, A.R. Chezan, M.H. Siekman, J.C. Lodder, D.O. Boerma and L. Niesen, J.Magn.Magn.Mater **240**, 423 (2002)
7. J.F. Bobo, H. Chatbi, M. Vergnat, L. Hennet, O. Lenoble, Ph. Bauer, M. Piecuch, J. Appl. Phys. **77**, 5309, (1995)
8. A.R. Chezan, C.B. Craus, N.G. Chechenin, T. Vystavel, J.Th.M. De Hosson, L. Niesen and D.O. Boerma, *IEEE Transaction on Magnetics*, v **38** no.5, 3144, (2002).
9. D. Pain, M. Ledieu, O. Acher, A.L. Adenot, F. Duverger, J. Appl. Phys. **85**, 5151, (1999)
10. J. Huijbregtse, F. Roozeboom, J. Sietsma, J. Donkers, T. Kuiper, and E. van de Riet, J. Appl. Phys. **83**, 1569 (1998)
11. S. Chikazumi, Physics of Ferromagnetism, Oxford University Press (1999)
12. D. Grünberg, C.M. Mayr, W. Vach, and M. Grimsditch, J.Magn. Magn.Mater. **28**, 319 (1982)
13. G. Suran, M. Naili, and M. Rivoire, J. Appl. Phys. **67**, 5649 (1990)
14. E van de Riet, W. Klaassens, F. Roozeboom, J.Appl.Phys, **81**, 806 (1997)
15. N.X. Sun, S.X. Wang, T.J. Silva, and A. Kos, IEEE Trans. on Magn. **38**, 146 (2002)
16. J.F. Cochran, R.W. Qiao, B. Heinrich, Phys. Rev. B. **39**, 4399 (1989)
17. M.J. Hurben, C.E. Patton, J. Appl. Phys. **83**, 4344, (1998)
18. H. Hoffmann, Phys. Stat. Sol. **33**, 175 (1969)
19. C.B. Craus, A.R. Chezan, D.O. Boerma, and L. Niesen, "The influence of the surface roughness on high frequency behavior of soft ferromagnetic thin films", to be submitted
20. W.M. Saslow, Phys. Rev. Lett. **50**, 1320 (1983)
21. W.M. Saslow, Phys. Rev. B **35**, 3454 (1987)

22. G.S. Gargill and T. Mizoguchi, J. Appl. Phys. **49** (1978) 1753
23. J.P. Jamet and A.P. Malozemoff, Phys. Rev. B **18**, 75 (1978)